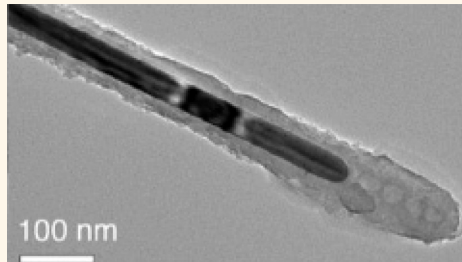


Silver Nanowire Exposure Results in Internalization and Toxicity to *Daphnia magna*

Leona D. Scanlan,[†] Robert B. Reed,[‡] Alexandre V. Loguinov,[†] Philipp Antczak,[§] Abderrahmane Tagmount,[†] Shaul Aloni,[⊥] Daniel Thomas Nowinski,[†] Pauline Luong,[†] Christine Tran,[†] Nadeeka Karunaratne,[†] Don Pham,[†] Xin Xin Lin,[†] Francesco Falciani,[§] Christopher P. Higgins,^{||} James F. Ranville,[‡] Chris D. Vulpe,^{†,*} and Benjamin Gilbert[†]

[†]Department of Nutritional Sciences and Toxicology, University of California Berkeley, 119 Morgan Hall, Berkeley, California 94720, United States, [‡]Department of Chemistry and Geochemistry, Colorado School of Mines, 1500 Illinois Street, Golden, Colorado 80401, United States, [§]Institute of Integrative Biology, University of Liverpool Centre for Computational Biology and Modeling, Crown Street, Liverpool L69 7ZB, United Kingdom, [⊥]Materials Sciences Division, Molecular Foundry, Lawrence Berkeley National Laboratory, 1 Cyclotron Road, MS 90-1116, Berkeley, California 94720, United States, ^{||}Department of Civil and Environmental Engineering, Colorado School of Mines, Golden, Colorado 80401, United States, and [¶]Earth Science Division, Lawrence Berkeley National Laboratory, Earth Sciences Division, 1 Cyclotron Road, MS 74-316C, Berkeley, California 94720, United States

ABSTRACT Nanowires (NWs), high-aspect-ratio nanomaterials, are increasingly used in technological materials and consumer products and may have toxicological characteristics distinct from nanoparticles. We carried out a comprehensive evaluation of the physicochemical stability of four silver nanowires (AgNWs) of two sizes and coatings and their toxicity to *Daphnia magna*. Inorganic aluminum-doped silica coatings were less effective than organic poly(vinyl pyrrolidone) coatings at preventing silver oxidation or Ag⁺ release and underwent a significant morphological transformation within 1 h following addition to low ionic strength *Daphnia* growth media. All AgNWs were highly toxic to *D. magna* but less toxic than ionic silver. Toxicity varied as a function of AgNW dimension, coating, and solution chemistry. Ag⁺ release in the media could not account for observed AgNW toxicity. Single-particle inductively coupled plasma mass spectrometry distinguished and quantified dissolved and nanoparticulate silver in microliter-scale volumes of *Daphnia magna* hemolymph with a limit of detection of approximately 10 ppb. The silver levels within the hemolymph of *Daphnia* exposed to both Ag⁺ and AgNW met or exceeded the initial concentration in the growth medium, indicating effective accumulation during filter feeding. Silver-rich particles were the predominant form of silver in hemolymph following exposure to both AgNWs and Ag⁺. Scanning electron microscopy imaging of dried hemolymph found both AgNWs and silver precipitates that were not present in the AgNW stock or the growth medium. Both organic and inorganic coatings on the AgNW were transformed during ingestion or absorption. Pathway, gene ontology, and clustering analyses of gene expression response indicated effects of AgNWs distinct from ionic silver on *Daphnia magna*.



KEYWORDS: silver · nanowire · ecotoxicology · *Daphnia magna* · acute toxicity · transcriptomics · single-particle inductively coupled plasma mass spectrometry

The volume and diversity of manufactured nanomaterials (NMs) are rapidly growing. One active area of nanoscience research and commercialization involves the design and fabrication of nanowires composed of metals, including silver, or semiconductors, including zinc oxide and silicon. Nanowires (NWs) are high-aspect-ratio NMs, longer in one dimension as a result of preferential growth during synthesis. NWs will have diverse roles in applications for which highly anisotropic physical properties are required, such as solar energy

capture, electrically active fabrics and tissues, and as composite materials.¹ Controlling the NW diameter can tune physical properties such as the optical band gap of semiconductors or the surface plasmon resonance frequency of metals.² Silver nanowires (AgNWs) are of particular interest for transparent flexible electrodes and heat shielding.^{3–5}

NMs from commercial products can be released into the environment during manufacture, use, or disposal,^{6,7} and consequently, there is considerable effort to

* Address correspondence to vulpe@berkeley.edu.

Received for review July 5, 2013 and accepted October 5, 2013.

Published online October 05, 2013
10.1021/nn4034103

© 2013 American Chemical Society

anticipate the environmental fate and toxicity of a range of nanomaterials, including AgNMs.^{8,9} However, relatively little work focuses on the specific impacts of NWs *versus* other nanomaterial types on ecological or biological toxicology. Decades of research on asbestos-causing minerals, and more recent studies of carbon nanotubes,^{10,11} demonstrated that high-aspect-ratio particles can be actively absorbed into cells both *in vitro* (cell culture) and *in vivo* (mouse) and may be biopersistent, resisting the action of macrophages to clear them from internal locations.¹² Cellular uptake of large NMs, including NP aggregates,¹³ CNTs,^{14,15} and NWs,^{16–18} is clearly documented. AgNW¹⁹ and ZnO-NW uptake²⁰ in mammalian cells has also been seen. CNT (and by extension, NW) uptake is believed to be caused by physical stimulation of a protein receptor, which initiates membrane wrapping of the NM.¹⁰

In studies of Ag nanoparticle toxicity, silver oxidation and ionic silver (Ag^+) release were typically identified to be at least partly responsible for the toxicity of AgNPs.^{21,22} However, it is unknown whether the molecular mechanisms of Ag^+ , AgNP, or AgNW toxicity are the same. To date, five articles have been published on the toxicity of AgNWs. Schinwald *et al.* studied AgNW length effect on immune response in mice and found a threshold to toxicity, below which shorter particles did not elicit a response.^{23,24} Schinwald also looked at frustrated phagocytosis of AgNW in mice *in vivo*.²⁵ Verma *et al.* tested AgNWs and AgNW films on four mammalian cell lines and found that wires alone were more toxic than thin film NW constructs and that toxicity was time-, dose-, and length-of-wire-dependent.¹⁹ They also observed the induction of autophagy by AgNWs in phagocytic cells. George *et al.* looked at the effects of AgNWs, nanospheres and nanoplates on fish epithelial cells and embryos.²⁶ In this system, AgNWs were less toxic than nanoplates, and toxicity was not only caused by Ag^+ release. None of these contributions established a AgNW LD or LC₅₀ value for comparative analysis of toxicity.

Work on other high-aspect-ratio NMs is also limited. Nanofibers may be absorbed into lysosomes or endosomes in human or mouse cells.^{16,27,28} The acute toxicity of $\alpha\text{-Fe}_2\text{O}_3$ -NW is low,¹⁶ while ZnO-NWs are as toxic to human monocyte macrophages as ZnNP and Zn^{2+} .²⁰ Through the development of libraries of metal oxide nanomaterials of varying dimensions, Meng *et al.* and Ji *et al.* found aspect ratio an important factor in uptake and toxicity of silica and CeO_2 nanofibers.^{18,28}

Here we report the toxicity of four types of AgNWs to *Daphnia magna*, an aquatic organism and an indicator of freshwater ecology and toxicity. As summarized in Table 1, we studied four types of AgNWs (two sizes and two coatings). The mean dimensions of the AgNWs were either 2 μm (length) \times 30 nm (diameter) or 20 μm \times 60 nm, referred to as “short” (S) or “long” (L) NWs,

TABLE 1. Summary of AgNW Samples^a

| name | dimensions | coating | % impurity nanorods |
|------------------------|--------------------------------------|------------------|---------------------|
| L-PVP-NW | 65 nm \times 20 μm long | PVP | 1.6 |
| L-SiO ₂ -NW | 65 nm \times 20 μm long | SiO ₂ | 0.8 |
| S-PVP-NW | 30 nm \times 2 μm short | PVP | <0.1 |
| S-SiO ₂ -NW | 30 nm \times 2 μm short | SiO ₂ | <0.1 |

^a PVP: poly(vinyl pyrrolidone) coating. SiO₂: amorphous aluminum-doped silica coating. Percent impurity: the percent of silver contributed by nanorod contaminants to each stock solution.

respectively. The coatings were either organic poly(vinyl pyrrolidone) (PVP) or inorganic, aluminum-doped silica (SiO₂). Silica coatings have been shown to prevent release of metal ions from nanomaterials^{29,30} and were expected to minimize the contribution of media-dissolved Ag^+ to toxicity. Toxicity studies were performed in one of two simulated freshwater media, “COMBO” or “EPA”. Abiotic studies of the physical and chemical stability of the nanowires were performed to test whether AgNW transformations in the media could explain trends in the toxicity data. The acute toxicity data were complemented by gene expression analyses.

The hypothesis that AgNWs entered the hemolymph, the major fluid-phase component of the *Daphnia* open circulatory system, was tested with single-particle inductively coupled plasma mass spectrometry (spICPMS) by quantifying the concentration of silver in hemolymph extracted from daphnids exposed to ~2 μm long AgNWs. spICPMS can achieve detection of parts per trillion (ppt) or parts per billion (ppb) concentrations of nanoscale particles in complex aqueous media.³¹ Recent studies on spICPMS focused on developing the technique for analysis of a range of nanomaterials such as silver,^{32,33} cerium and titanium oxides,³⁴ and carbon nanotubes.³⁵ Environmental and biological applications of spICPMS include analysis of wastewater plant effluent^{32,33} and quantification of DNA after attachment to gold nanoparticles.³⁶ To the best of our knowledge, the present work is the first to quantify NMs in microliter volumes of a biological fluid. Scanning electron microscopy (SEM) provided direct observation and morphological characterization of AgNMs with either SiO₂ or poly(vinyl pyrrolidone) (PVP) coatings extracted from the hemolymph. Dark-field optical microscopy of daphnids exposed to PVP-coated NWs was used to study routes of AgNW entry and to investigate bioaccumulation.

RESULTS

Physicochemical Characterization. Characterization of the four AgNW preparations with transmission electron microscopy (TEM) imaging found both AgNWs and silver nanorods (NR) approximately 100 nm \times 500 nm (Supporting Information Figure S1) in the long NW samples, which likely represents incomplete

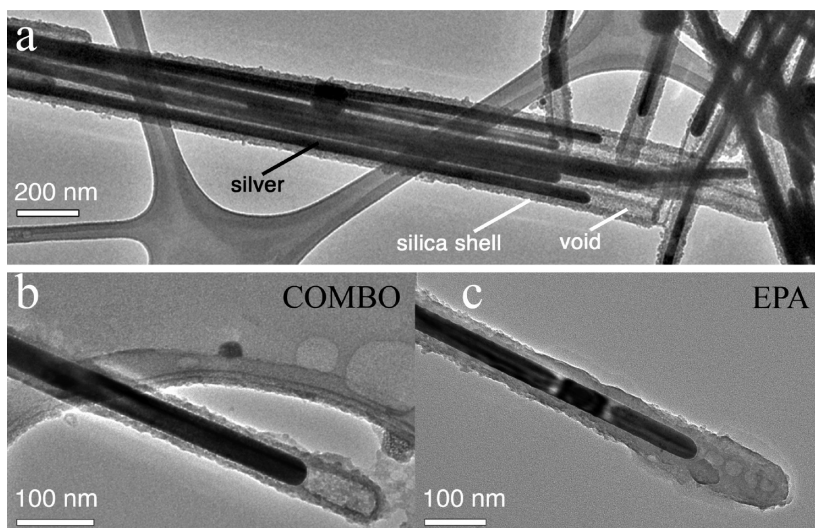


Figure 1. TEM study of the morphology of the aluminosilicate coating on (a) as-synthesized S-SiO₂-NWs, or following a 2 h exposure to (b) COMBO or (c) EPA media. Other representative micrographs showing morphological changes in the S-SiO₂-NW exposed to EPA media are given in Figure 2 and Figure S4.

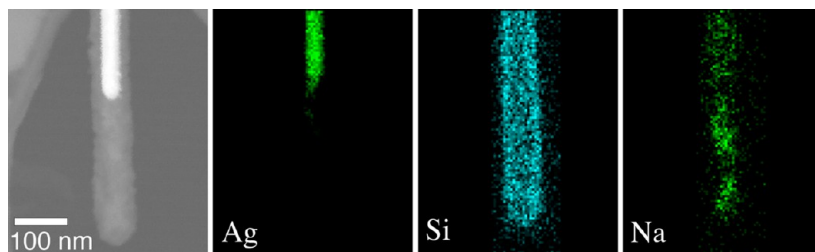


Figure 2. STEM study of S-SiO₂-NWs following exposure to EPA medium. Left panel shows the STEM image; other panels show corresponding elemental maps depicting the distribution of silver (Ag), silicon (Si), and sodium (Na).

synthesis products. No nanorods were detected in short NW stock suspensions. NR contamination was 1.6% in L-PVP-NW and 0.8% in L-SiO₂-NW (Tables 1 and S1). Assessment of AgNW behavior in aqueous solution found all AgNWs dispersed without aggregation in pure water. PVP-NWs were stable in both *Daphnia* growth media, but SiO₂-NWs aggregated in both media, with concomitant increase in settling rates (Figures S2 and S3). The ζ -potentials for S-PVP-NW and S-SiO₂-NW in ultrapure water were -18 and -32 mV, respectively, in agreement with prior measurements^{37,38}. Long NWs could not be analyzed. The ζ -potentials in growth media were zero, indicating complete electrolyte shielding of the surface charge and explaining the aggregation of the SiO₂-NW observed.

SEM imaging did not find any morphological changes in PVP-NW exposed to any media. Morphological changes in SiO₂ coatings did not occur in COMBO media but did occur after a few hours exposure to EPA media (Figure 1a,b). The most evident change was loss of the space (void) between coating and metal at the tips, which were present in the original AgNWs. Although some porosity may remain (Figure 1c), the morphology of silica at the SiO₂-NW tip for all observed SiO₂-NWs (Figures 1c, 2, and S4) is clearly distinct from

the original (Figure S5). Figures 1c and 2 show TEM and elemental imaging of a SiO₂-NW in EPA media. The silica distribution shows evidence of a diffuse network extending out from the surface of the NW. The sodium distribution shows accumulation of Na⁺ in a pattern consistent with diffusion into the silica, indicating that the surface coating became porous.

Ionic Silver Release into Media. Ag⁺ release was detected only in the following samples: S-SiO₂-NW in water and in COMBO and EPA media and S-PVP-NW in EPA media (Figure 3). No other AgNW released detectable Ag⁺ in any solution. COMBO and EPA media components are listed in Table S2. Silver speciation calculations of Ag⁺ complexation by anions, principally Cl⁻ (Table S3), predicted a greater percentage of free Ag⁺ in EPA (84%) than COMBO (41%).

Acute Toxicity. The acute 24 h LC₅₀ values for AgNWs and Ag⁺ in COMBO or EPA media range from 3.6 to 522 μ g silver per liter media (μ g/L) (Figure 4 and Table S4). The LC₅₀ values were significantly different between all samples except for Ag⁺ in COMBO versus Ag⁺ in EPA and L-PVP-NW in COMBO versus L-SiO₂-NW in EPA, determined by comparing the log(LC₅₀) and confidence interval ratio) to 0 for each pair of values.³⁹ The toxicity of Ag⁺ was greater than toxicity of any AgNWs in either

media. S-SiO₂-NW was the most toxic AgNW to *Daphnia* in both media. We found three trends related to toxicity: short wires were more toxic than long; SiO₂ coating was more toxic than PVP; and exposures in EPA media were more toxic than those in COMBO. However, there is one exception: L-PVP in COMBO was more toxic than L-SiO₂ in COMBO, L-PVP in EPA, and S-PVP in COMBO.

Unique Gene Expression Profiles and Potentially Unique Modes of Toxicity. A total of 2801 genes were identified as differentially expressed gene candidates (Table 2). Gene expression response was not correlated to LC₅₀ (data not shown). Ag⁺ caused the most robust response, followed by S-PVP-NW and then SiO₂-NW. L-PVP-NW resulted in fewest candidate genes and was also the only exposure with more up-regulated than down-regulated genes. Only seven genes were common to all conditions (Figure S6). The qPCR results

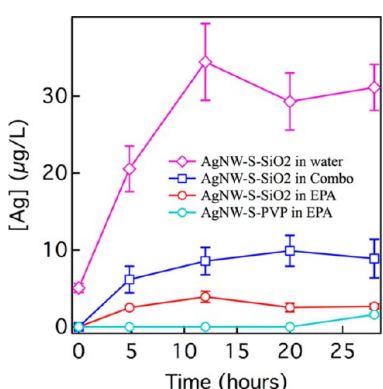


Figure 3. Determination of relative rates of release of Ag⁺ by long (L) and short (S) AgNWs at a silver concentration of 111 μM in water and in *Daphnia* media. Silver was undetectable for S-PVP-NWs in COMBO and water and for all L-NW samples. Ag⁺ was defined as the fraction passing through a 0.2 μm filter. The main source of error is Ag⁺ retention in the filter. To represent the magnitude of this uncertainty, the plot contains error bars that are the standard deviations on individual measurements of the second, third, and fourth 1 mL portions of the filtrate passed through the same filter.

on seven genes (Table S5, representing 12 qPCR reactions) correlated with microarray results, with one exception (Table S6). The microarray data are available in Table S7 and have been deposited in NCBI's Gene Expression Omnibus (Edgar *et al.*) and are accessible through GEO Series accession number GSE47064 (<http://www.ncbi.nlm.nih.gov/geo/query/acc.cgi?acc=GSE47064>).⁴⁰ We analyzed the differential gene expression (DGE) of genes encoding sodium–potassium adenosine triphosphatase (Na⁺/K⁺ ATPase) proteins because Ag⁺ toxicity to *Daphnia* is traditionally attributed to inhibition of these cellular transport proteins in the gill.^{41–43} All 1/10 LC₅₀ exposures affected ion transport (Table S8), but Ag⁺ caused the strongest response. Transporter expression decreased in all exposures, except L-SiO₂-NW caused an increase in an iron(III) dicitrate transporter. Ag⁺ significantly suppressed the expression of a calcium-transporting ATPase (with only 11% expression relative to control) and an ABC-related transporter (27%). It is unknown whether these are sodium transporters.

HOPACH analysis of gene expression data clustered the silver exposures into three distinct groups (Figure 5). Similarity of gene expression profile is color-coordinated, with darker gray most similar and white least similar. Gene expression profiles for S-PVP-NW, S-SiO₂-NW, and Ag⁺ were similar enough to group in one cluster, evident by dark coloring in the HOPACH diagram and by the numbered labeling on the x-axis (cluster 3). The L-NW each clustered uniquely (clusters 1 and 2).

TABLE 2. Numbers of Genes Differentially Expressed in AgNW and Ag⁺ Exposures As Compared to Control^a

| # DEG | L-PVP | L-silica | S-PVP | S-silica | silver |
|-------|-------|----------|-------|----------|--------|
| up | 143 | 212 | 121 | 182 | 182 |
| down | 134 | 307 | 502 | 381 | 510 |
| total | 277 | 519 | 623 | 563 | 692 |

^a Numbers represent number of statistically significant candidate differentially expressed genes for each exposure condition.

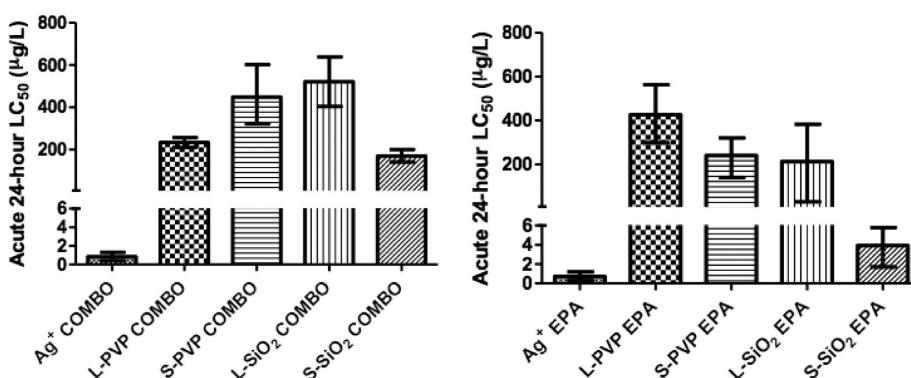


Figure 4. Acute 24 h LC₅₀ values for AgNW and Ag⁺ on *Daphnia magna* in (a) COMBO and (b) EPA media. LC₅₀ values are measured in micrograms silver per liter (μg/L). LC₅₀ values and 95% confidence intervals were determined with probit analysis. A table of LC₅₀ values is found in Table S4. Statistical analysis of LC₅₀ values showed that the LC₅₀ values for each AgNW in both media were significantly different. LC₅₀ values for Ag⁺ were not significantly different between the two media.

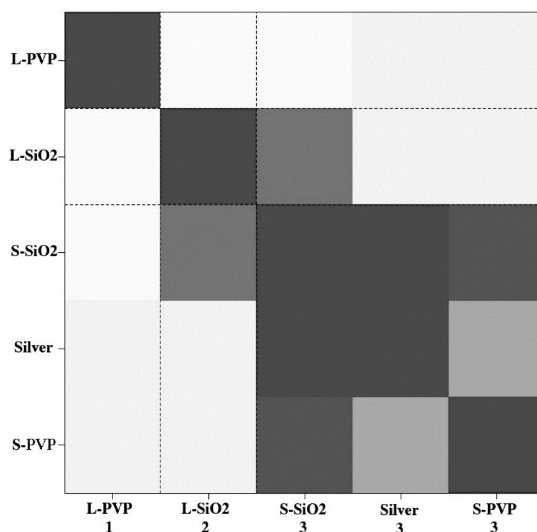


Figure 5. Hierarchical ordered partitioning and collapsing hybrid (HOPACH) analysis of gene expression data from AgNW-exposed *versus* media-only control daphnids. HOPACH clustered data into three groups based on similarity of gene expression profile. Groups are labeled on the x-axis as 1 (L-PVP-NW), 2 (L-SiO₂-NW), or 3 (S-SiO₂-NW, Ag⁺, and S-PVP-NW).

TABLE 3. KEGG Pathway Analysis of Gene Expression Data from *Daphnia magna* Exposed to AgNWs Identified the Enrichments of Different Biological Pathways^a

| affected biological pathway | L-PVP | L-SiO ₂ | S-PVP | silver |
|----------------------------------------------|-------|--------------------|-------|------------------------|
| oxidative phosphorylation | | | | 5.3 × 10 ⁻⁴ |
| spliceosome | 0.02 | | | |
| peroxisome | | 0.02 | | |
| lysosome | | 0.04 | | |
| ribosome | 0.01 | | 0.01 | 1.8 × 10 ⁻⁴ |
| progesterone-mediated oocyte maturation | | 0.01 | | |
| metabolism of xenobiotics by cytochrome P450 | | 0.02 | | |
| drug metabolism - cytochrome P450 | | 0.03 | | |
| retinol metabolism | | 0.05 | | |

^aThe *p* values 0.05 or less were considered significant. KEGG analysis on S-SiO₂-NW data found no statistically significant results.

Kyoto Encyclopedia of Genes and Genomes (KEGG) pathway analysis found at least one enriched pathway in each exposure condition except S-SiO₂-NW (Table 3). L-SiO₂-NW affected the largest number of pathways including cytochrome P450 xenobiotic metabolism, peroxisome, and lysosomal pathways. PVP-NWs and Ag⁺ affected ribosomal pathways, the only in-common effect for any exposure, and L-PVP-NW affected spliceosomal pathways. Ag⁺ exposure caused the most statistically significant pathway changes in oxidative phosphorylation and ribosomal pathways. An increase in rRNA expression was confirmed for Ag⁺ exposure by independent qPCR analysis of the ribosomal 18S subunit.

GO ontology enrichment analysis of gene expression data using Blast2GO⁴⁴ (B2G) showed significant

TABLE 4. Blast2GO Analysis Shows Significant Enrichment of Functional Gene Groups PVP-NW and Ag⁺ Exposures

| enriched molecular function ^a | exposure condition |
|--------------------------------------------------------------|-----------------------------------------|
| structural constituent of cuticle (GO:0042302) | L-SiO ₂ , S-SiO ₂ |
| structural molecule activity (GO:005198) | L-SiO ₂ , silver |
| structural constituent of ribosome (GO:0003735) | silver |
| ribosome biogenesis (GO:0042254) | silver |
| ribosome (GO:0005840) | silver |
| ribonucleoprotein complex biogenesis (GO:0022613) | silver |
| cellular component biogenesis at cellular level (GO:0071843) | silver |
| ribonucleoprotein complex (GO:0030529) | silver |
| cytosolic ribosome (GO:0022626) | silver |

^a GO: term corresponds to the gene ontology identification in Blast2GO.

over-representation of molecular function ontologies for both SiO₂-NW exposures and for Ag⁺ (Table 4). Specifically, L-SiO₂-NW showed changes in an unnamed structural component also affected by Ag⁺; Ag⁺ also changed ribosomal function and ribosomal biogenesis, and both SiO₂-NWs caused a change in expression of cuticle (carapace) structure genes. No significant results were found for PVP-NW. Further details on B2G results are found in Table S9.

spICPMS Analysis—AgNW Exposures. No dissolved silver was detected by any method in growth medium or hemolymph fluid from daphnids in any control experiments. Preliminary abiotic trials of AgNW detection and quantification by spICPMS were performed by adding 155 μg Ag/L S-SiO₂-NW to COMBO medium and sampling at three time points (0, 24, and 48 h). The distribution of AgNW size in the medium calculated from spICPMS measurements is given in Figure S7. Over the 48 h period, we observed a drop in particle number without a change in calculated particle dimensions or in dissolved Ag⁺. This is in agreement with our observations that AgNWs settle at a detectable rate in the growth medium.

Particulate silver consistent with AgNWs was detected by spICPMS analysis of silver in the hemolymph taken from a daphnid exposed to ~2 μm L-SiO₂-NW at the LC₅₀ concentration (Figure 6). Dissolved silver, including free Ag⁺ and inorganic and biological complexes of the silver ion, contributes a constant background signal, while silver-rich particles result in pulses in the ICPMS response.³² Concentrations of dissolved and particulate silver are distinguished by selecting an intensity cut-off in ICPMS response that is depicted by the blue lines in the raw data (Figure 6a) and in the ICPMS response histogram (Figure 6b). The cut-off represents an intensity above which the signal is determined to be a discrete pulse (*i.e.*, a particle), whereas intensities below this value represent dissolved silver and silver NPs having an equivalent spherical diameter smaller than about 30 nm. In this study, a cut-off of >3 standard deviations above an average of the background intensities was used to

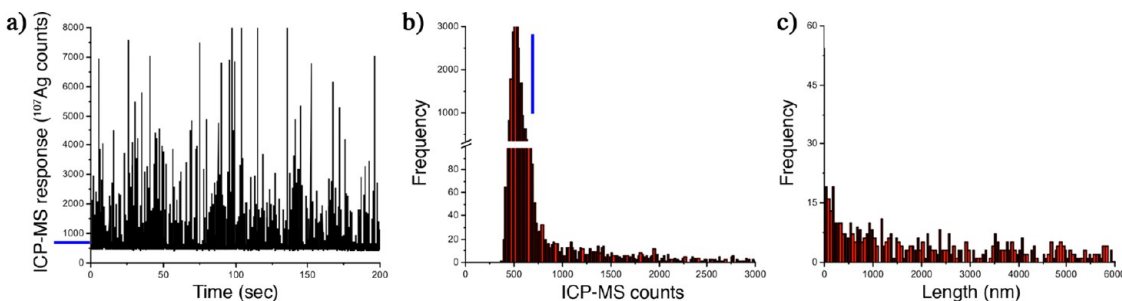


Figure 6. Single-particle inductively coupled plasma mass spectrometry (spICPMS) quantification of dissolved and particulate silver in the hemolymph of a daphnid exposed to $\sim 2 \mu\text{m}$ long silica-coated silver nanowires (AgNWs) at the LC₅₀ concentration ($155 \mu\text{g Ag/L}$). (a) Raw data. (b) Histogram of detector response. (c) Calculated AgNW length distribution. Blue lines in (a) and (b) represent the cut-off in spICPMS response used to distinguish the signal from dissolved and particulate silver.

TABLE 5. spICPMS Analysis of Daphnia Exposure to Silver Nanowires^a

| silver concentration used | | | | | | |
|---------------------------|--------------------------------------------------------|------------------|----------------------------|-----------------------------------|-----------------------------------|---------------------------------------|
| sample | (LC ₅₀ = $155 \mu\text{g/L}$) ^b | presence of food | sampling time ^c | dissolved Ag (ppb) ^{d,e} | particulate Ag (ppb) ^f | particle number (mL^{-1}) |
| growth medium | 10% LC ₅₀ | yes | predep | 0.071 ± 0.03 | 0.16 ± 0.005 | $1.5 \times 10^4 \pm 2.3 \times 10^2$ |
| growth medium | 10% LC ₅₀ | no | predep | 0.140 ± 0.04 | 0.12 ± 0.005 | $9.9 \times 10^3 \pm 3.7 \times 10^2$ |
| growth medium | 10% LC ₅₀ | no | postdep | 0.040 ± 0.02 | 0.015 ± 0.001 | $9.7 \times 10^3 \pm 1.1 \times 10^3$ |
| hemolymph | 10% LC ₅₀ | yes | postdep | | 17.4 ± 0.2 | $3.6 \times 10^6 \pm 1.5 \times 10^5$ |
| hemolymph | 10% LC ₅₀ | no | postdep | | 10.8 ± 0.4 | $2.9 \times 10^6 \pm 6.2 \times 10^4$ |
| hemolymph | LC ₅₀ | yes | predep | 479 ± 154 | 405 ± 102 | $4.5 \times 10^7 \pm 5.7 \times 10^6$ |

^a spICPMS analysis of dissolved and particulate silver in Daphnia growth medium and hemolymph following exposure to short ($\sim 2 \mu\text{m}$ long) silica-coated AgNWs at the conditions indicated. ^b LC₅₀ for S-SiO₂-NW in COMBO is $155 \mu\text{g/L}$ (155 ppb). ^c Samples were collected before or after a 1.5 h depuration period in silver-free medium. ^d Omitted values were below the effective detection limit, estimated to be 10 ppb in hemolymph (accounting for dilution from several microliters up to a sufficient volume, 5–10 mL, for spICPMS analysis). ^e Errors on dissolved Ag were calculated for each sample from the variation in the dissolved Ag signal throughout the measurement, expressed as \pm one standard deviation. ^f Particulate Ag mass concentration calculations were performed by integrating the masses calculated from all pulse events in a single spICPMS analysis and dividing by the volume analyzed. Error is \pm one standard deviation from duplicate samples.

make this distinction. The particle size (length) distribution calculated from the particulate signal from the hemolymph is given in Figure 6c and details a shift to smaller particles than those found in the medium (Figure S7).

We further quantified dissolved and particulate silver in the medium and hemolymph for a range of experimental conditions using spICPMS (Table 5). Media were analyzed after exposure to 1/10 LC₅₀ of S-SiO₂-NW ($15.5 \mu\text{g/L}$). Samples were taken before a depuration period with or without feeding and after a depuration period without feeding. Hemolymph analysis was done at 1/10 LC₅₀ after a depuration period with and without feeding and at the LC₅₀ with no depuration period. We detected particulate silver in the hemolymph of daphnids for all AgNW exposure conditions and in all samples and replicates. S-SiO₂-NW exposures were performed at two silver concentrations (the LC₅₀ and 1/10 LC₅₀), with and without food added to the AgNW-containing media, and with or without a 1.5 h depuration period in AgNW-free media in order to permit gut clearance. These comparisons indicate that particulate silver was not manually transferred from the gut into the hemolymph during extraction. At the 1/10 LC₅₀ exposure, dissolved Ag⁺

in hemolymph fluid was below the detection limit (~ 10 ppb in the hemolymph, accounting for the 1000× dilution factor required for analysis). However, at the LC₅₀ exposure, the levels of both Ag⁺ (479 ppb) and particulate silver (405 ppb) in the hemolymph exceeded the initial AgNW concentration in the media (155 ppb).

SEM Imaging of Daphnia Hemolymph. SEM analysis of dried hemolymph provided independent evidence that AgNWs migrated from the media into the daphnid interior. Figure 7 shows scanning electron microscopy images of AgNWs with two types of surface coatings that were located in dried *Daphnia* hemolymph. The SEM images reveal evidence of surface modifications not observed for AgNWs exposed to COMBO growth medium alone. PVP-NWs (Figure 7a) appeared to be coated by a filamentous organic material, indicating either partial loss of the polymer coating or adhesion of organic matter. The oxide shell surrounding the silica-coated AgNWs was completely removed (Figure 7b). Although restructuring of the silica coating was observed in lower ionic strength growth medium (Figures 1c, 2, and S4), it did not occur in COMBO media. Thus, the surface modifications likely occurred within the organism.

SEM imaging also located silver-rich precipitates, in addition to AgNWs, in the hemolymph (Figures 7b and S8a). The size and morphology of these precipitates differ from trace silver nanocrystals present in some stock solutions (Figure S5), indicating that new nanoparticles had precipitated during the experiment. Energy-dispersive X-ray (EDX) analysis (Figure S8b) identified only silver, oxygen, and silicon from the substrate, suggesting the precipitate to be a silver oxide. EDX analyses of smaller precipitates and AgNWs also revealed sodium and chlorine, likely physiological ions from the hemolymph. SEM analysis located at least one AgNW in the hemolymph of daphnids exposed to all types of AgNWs at the respective LC₅₀ concentrations. However, AgNW uptake could not be reliably quantified by SEM. Moreover, AgNWs or particulate silver were not detectable by SEM imaging in hemolymph from daphnids exposed at the 1/10 LC₅₀

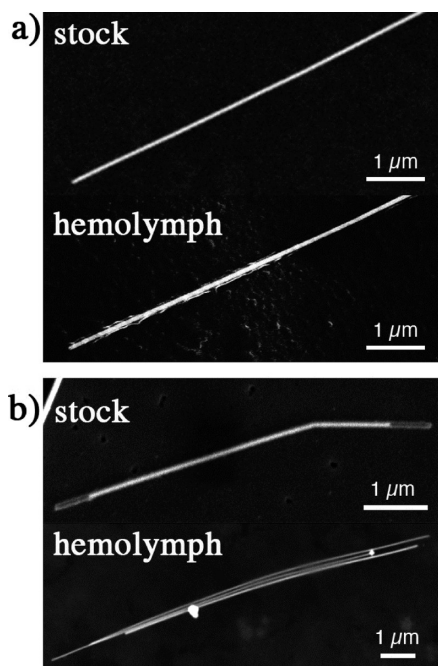


Figure 7. Scanning electron microscope images of comparing AgNWs taken from stock suspension and located in *Daphnia* hemolymph. (a) PVP-coated AgNW. (b) Silica-coated AgNW.

concentration. In contrast, the more sensitive spICPMS technique readily detected silver nanomaterials in hemolymph at the 1/10 LC₅₀ dose (Table 5).

spICPMS Analysis—Ag⁺ Exposure. spICPMS analyses of dissolved and particulate silver in growth medium and in hemolymph for Ag⁺ exposures at 1/10 LC₅₀ and the LC₅₀ measured for AgNO₃ ($0.8 \pm 0.4 \mu\text{g/L}$) are reported in Table 6. At 1/10 LC₅₀, no silver was detectable in the hemolymph. At the LC₅₀ value, only particulate Ag was detected in the hemolymph at a level (3.3 ppb) that exceeded the initial dissolved Ag concentration in the medium (0.8 ppb). Figure S9 reports the mass distribution of particulate silver. SEM imaging could not detect silver-rich precipitate in dried hemolymph in these samples.

Dark-Field Optical Microscopy. Although the diameter of all AgNWs used in this study were significantly below the resolution of optical microscopy, AgNPs⁴⁵ and pristine AgNWs (Figure S10a) are detectable as bright features when imaged by dark-field microscopy. Dark-field imaging of live daphnids exposed to AgNWs revealed freely diffusing AgNWs in the rostrum, in the post-abdominal region by the anus, and inside the brood chamber in which eggs are hatched (Figures S11–S13). AgNWs were also identified adhering to the exterior of the organism including in the vicinity of the gills. Relatively few individual AgNWs were identified in the gut. However, the alimentary canal of daphnids exposed to AgNWs appeared much brighter than for control animals (Figure S14), suggesting an aggregated mixture of food and silver materials.

DISCUSSION

The LC₅₀ data in Figure 4 and Table S4 show that all AgNWs can be classified as highly toxic to aquatic organisms as they exhibit LC₅₀ values below 1 mg/L.⁴⁶ Short and SiO₂-coated AgNWs and exposures done in EPA media were usually more toxic than long and PVP-coated wires or exposures in COMBO media. However, the toxicity of all AgNWs is significantly less than that of Ag⁺ (AgNO₃). AgNWs also appear to exert less toxicity than Ag nanoparticles. Poynton *et al.* studied the toxicity of 35 nm diameter PVP-coated AgNPs on 10 day

TABLE 6. spICPMS Analysis of *Daphnia* Exposure to Ionic Silver^a

| sample | silver concentration ^b | presence of food | sampling time ^c | dissolved Ag (ppb) ^{d,e} | particulate Ag (ppb) ^{d,f} | particle number (mL ⁻¹) |
|---------------|-----------------------------------|------------------|----------------------------|-----------------------------------|-------------------------------------|---------------------------------------|
| growth medium | 10% LC ₅₀ | yes | predep | 0.019 ± 0.03 | | |
| hemolymph | 10% LC ₅₀ | yes | predep | | | |
| growth medium | LC ₅₀ | yes | predep | 0.092 ± 0.02 | 0.028 ± 0.001 | $1.9 \times 10^4 \pm 1.5 \times 10^2$ |
| hemolymph | LC ₅₀ | yes | predep | | 3.13 ± 0.2 | $1.4 \times 10^7 \pm 1.0 \times 10^5$ |

^a spICPMS analysis of dissolved and particulate silver in *Daphnia* growth medium and hemolymph following exposure to ionic silver (as AgNO₃) at the exposure conditions indicated. ^b LC₅₀ for AgNO₃ in COMBO is $0.8 \mu\text{g/L}$ (0.8 ppb). ^c Samples were collected before or after a 1.5 h depuration period in silver-free medium. ^d Omitted values were below the effective detection limit, estimated to be 10 ppb in hemolymph (accounting for dilution from several microliters up to a sufficient volume, 5–10 mL, for ICPMS analysis). ^e Errors on dissolved Ag were calculated for each sample from the variation in the dissolved Ag signal throughout the measurement, expressed as \pm one standard deviation. ^f Particulate Ag mass concentration calculations were performed by integrating the masses calculated from all pulse events in a single spICPMS analysis and dividing by the volume analyzed. Error is \pm one standard deviation from duplicate samples.

old *Daphnia* in EPA media, finding LC₅₀ values to be ~10 µg/L.²² No PVP-NW was more toxic than this AgNP.

Other acute LC₅₀ values for Ag⁺ on *Daphnia magna* range from 0.39 µg/L for a 48 h exposure on 5 day old daphnids in purified lake water to 1.2 µg/L for a 48 h exposure on neonates in an "EPA"-like media.^{37,47} In *Daphnia magna*, toxic effects of silver are traditionally considered a function of the degree of saturation of biotic ligands by free Ag⁺.⁴¹ However, in related species *Ceriodaphnia dubia*, small complexes (thiosulfates, Ag-cysteine, Ag-Glut) are absorbed through amino acid/peptide transporters and also cause toxicity.⁴⁸ While there is more free Ag⁺ in the EPA media, the toxicity is not significantly increased from exposure in COMBO media, and phenomena contributing to this observation are unclear. Major conclusions of this work are presented and discussed below.

Physical Factors Cannot Explain Differences in AgNW Toxicity. Aggregation and settling can reduce toxicity.^{49–51} However, S-SiO₂-NWs were more toxic than S-PVP-NW even though S-SiO₂-NWs tended to aggregate and settle more. Further, there was no statistical difference between LD₅₀ values obtained with the *Daphnia* media shaken (to reduce AgNW settling) or still (Supporting Information Methods). Settling and aggregation therefore may not be dominant determinants in AgNW toxicity to *Daphnia magna*. Aggregated AgNWs could exhibit different uptake and toxicity than dispersed AgNWs, but this hypothesis was not tested in the present study. Settling of AgNWs may be irrelevant in *Daphnia* exposures as the animals move throughout the entire water column during exposure.

Long NW suspensions contained ~100 × 500 nm nanorod (NR) impurities at concentrations of 0.8 and 1.6% silver for L-SiO₂-NW and L-PVP-NW, respectively. Short NW contained <0.1%. While these nanorods may contribute to toxicity, they would have to be orders of magnitude more toxic than the AgNWs or 35 nm diameter NPs²² to account for the observed LD₅₀ values. The S-SiO₂-NWs (with no detectable nanorod contamination) are much more toxic than L-PVP-NWs (highest NR contamination), although the presence of NR could contribute to the increased toxicity of L-PVP-NWs. However, HOPACH analysis shows the long NWs with NR contamination on each cluster uniquely, indicating unique molecular effects, not an in-common mechanism. We conclude that the impurity NR represents a minor contribution to toxicity. This conclusion is in accord with nanofiber toxicity studies showing a high-aspect-ratio threshold to toxicity.^{11,28}

Chemical Processes Occurring in the Stock Suspensions or in the Media Cannot Fully Explain Trends in AgNW Toxicity. The content of Ag⁺ in stock (Table S1) and the Ag⁺ release rate between different AgNWs (Figure 3) varied considerably, with SiO₂-NWs being more reactive. This finding was surprising because the Al-doped SiO₂

coating was stable in the stock solution and was expected to completely encapsulate the silver.^{29,52} Figures 1 and 2 show that sodium ions penetrate into the SiO₂-NW coating when the SiO₂-NWs are dispersed in EPA media. This finding indicates that the coating is not an impervious barrier to media and could increase the NW toxicity by allowing Ag⁺ release.

Solution chemistry affected rates of oxidation and release, shown by the comparison of S-SiO₂-NWs in water, COMBO, and EPA (Figure 3). Precipitation of AgCl(s) does not explain the differences in measured silver ion release in these abiotic oxidation experiments because all solutions were undersaturated with respect to this phase. The data strongly indicate that there is a relationship between solution composition, morphological restructuring of the silica coating, and the rates of silver ion release into solution. However, no simple relationship could be uncovered. For example, although biogenic silica dissolution rate is observed to be enhanced in higher ionic strength solutions,⁵³ coating restructuring is observed only in the lower salinity EPA medium. Although the chemical stability of PVP-coated AgNWs is now well-understood,⁵⁰ the SiO₂–AgNM system is more complex, likely because Ag⁺ ions can sorb upon or within the silica coatings.

Although the trends in Figure 3 could not be fully explained, these empirical results could be used to estimate the contribution of Ag⁺ to AgNW toxicity. Because the release of Ag⁺ in media is proportional to the concentration of AgNWs, we predicted amounts of Ag⁺ at the AgNW LD₅₀ concentrations (Table S10). At the LD₅₀ for S-SiO₂-NWs in COMBO (155 µg/L), the calculated Ag⁺ concentration [Ag⁺(aq)] = 0.115 µg/L. This value is the highest amount of calculated Ag⁺ in media in any AgNW exposure and is only a fraction of the LD₅₀ for AgNO₃ in COMBO (0.8 µg/L). All other AgNW-released Ag⁺ concentrations are 10–1000 times less than the LD₅₀ for AgNO₃ (0.6–0.8 µg/L). This analysis indicates that AgNW are toxic to *Daphnia* through mechanisms other than Ag⁺ release into media. Although silver can form dissolved complexes with inorganic aqueous ions such as Cl[−], the calculated speciation of Ag⁺ in different media (Table S3) also does not explain trends in toxicity.

Different AgNWs Elicit Distinct Gene Expression Profiles in *D. magna*. Each AgNW gave a surprisingly distinct pattern of DGE with limited overlap between AgNWs of the same size or coating. There also were relatively low levels of common DGE among the AgNW samples and between each AgNW and AgNO₃. HOPACH cluster analysis, which visualizes patterns of gene expression independently of gene annotation, grouped the AgNWs based on similarity of DGE patterns (Figure 5). Results show S-PVP-NW and S-SiO₂-NW elicited the most similar response to Ag⁺ but were not completely identical.

KEGG pathway and GO ontology enrichment analysis found evidence for limited overlap in the effects of

the nanowires. KEGG pathway analysis revealed that only genes related to the ribosomal biological pathway were affected by more than one exposure type: L-PVP-NW, S-PVP-NW, and Ag⁺ (Table 3). These analyses were limited by the large number of unannotated genes on the *Daphnia* microarray. Nevertheless, published studies corroborate KEGG pathway results: Ag⁺ has been shown to affect ribosomal subunits in bacteria⁵⁴ and oxidative phosphorylation in rat liver.⁵⁵ While uncoated 40 and 80 nm AgNPs also effect oxidative phosphorylation,⁵⁶ no similar response was seen for any AgNW. In contrast, B2G ontological enrichment analysis indicated similar effects between L-SiO₂-NW and S-SiO₂-NW exposures and between L-SiO₂-NW and Ag⁺. These results point to a diverse range of biological end-points affected by exposure to different AgNWs. Specific mechanisms of toxicity are unclear, but data indicate a response to both internal Ag⁺ and to the AgNW itself.

Ionic Silver Exposure Leads to Nanoparticulate Silver Precipitation in the Hemolymph. The observation of internal nanoparticulate silver following ionic silver exposure is a novel finding that is not an experimental artifact of hemolymph extraction. Care was taken to avoid puncturing the gut epithelium or transferring AgNWs into the hemolymph. Animals were washed in fresh COMBO media before extraction to minimize AgNW contamination of pipet tips. Hemolymph extraction and dilution would not have caused the precipitation of silver-rich particles, as dilution in ultrapure water lowers the saturation state of the solution well beneath that of any common silver phase.⁵⁰ This finding adds to our knowledge of ionic silver toxicity. Ag⁺ ions that are not complexed to dissolved inorganic (e.g., chloride) or organic (e.g., cysteine) species can be transferred across cellular membranes by sodium transporters. Following Ag⁺ internalization, further reaction within the organism appears to lead to the formation of new silver-rich particles, possibly through reduction to form Ag⁰(s), salt formation, or complexation with biomolecules. The hyperaccumulation of Ag⁺, biological reduction, and subsequent precipitation as AgNPs has been documented for two plants, *Brassica juncea* and *Medicago sativa*,⁵⁷ and may represent a detoxification mechanism.

AgNWs Can Be Absorbed from Media into Hemolymph and Are Chemically Modified. DGE profiles showed biological effects of L-NWs to occur through mechanisms alternate to and in addition to Ag⁺. KEGG analysis also suggested exposure to L-SiO₂-AgNWs caused lysosomal activation, a common marker in high-aspect-ratio NM exposures^{18,27,58} and in aquatic species.⁵⁹ This observation could indicate frustrated phagocytosis or absorption into the animals and subsequent lysosomal activation. Regardless of mode of uptake, AgNW transfer into the organism was verified by hemolymph extraction, spICPMS quantification of nanoparticulate silver, and SEM observation of individual AgNWs with dramatically altered surface coatings.

Loss or transformation of surface coating may have facilitated AgNW oxidation and enhanced Ag⁺ generation within the organism. The contribution of released coating material to toxicity is unknown. However, SiO₂ coatings on metallic NMs, including silver NPs, typically reduce toxicity relative to bare NMs,^{29,52} and PVP is commonly used in pharmaceutical preparation and is found ubiquitously in the environment.⁶⁰ Chemical transformation of AgNW surfaces, such as exposure to fixative (Figure S10b), can cause loss of bright signal in dark-field mode and likely explains why dark-field imaging was not able to identify AgNMs within the hemolymph of daphnids. Dark-field imaging showed that surface transformations may have not occurred in the medium, the mouth, post-abdominal region, or brood hatch but may have occurred in the gut or following transfer (by any route) into the hemolymph. The pH of the *Daphnia* gut (pH 6–7.2⁶¹) is not high enough to cause the dissolution of the SiO₂ coating. However, in the present study, SiO₂ dissolution may be facilitated if absorption into the daphnids involved transfer to a more basic cellular compartment. Alternatively, the complex mixture of digestion enzymes in the gut could affect both organic and inorganic coatings, as was seen when lysophosphatidylcholine coatings on single-walled carbon nanotubes were chemically degraded following ingestion.⁶² Clearly, intraorganism biologically mediated surface alterations could significantly affect NM uptake and toxicity and warrant further study.

Mechanism of AgNW Uptake Is Unclear. It is generally accepted that the dominant route for NM uptake by aquatic organisms is *via* the gastrointestinal tract (gut), although the factors controlling the specific pathways and accumulation patterns for NMs are not well-understood. As reviewed by Jovanovic *et al.*,⁵⁹ NM exposure in fish can cause immunological responses in multiple cell types throughout an organism. TiO₂ NPs fed to rainbow trout were absorbed from the gut⁶³ and reached the liver, spleen, and brain.⁶⁴ In *Daphnia*, Rosenkranz *et al.* used a combination of fluorescence microscopy and electron microscopy to show that both 1 μm and 20 nm diameter polymer spheres could transfer from the gut into internal oil storage droplets.⁶⁵ Zhao *et al.* used radiolabeling to show that ~20 nm diameter AgNPs mixed with algae were retained in *Daphnia* with a lower rate of efflux than Ag⁺ and concluded that a significant portion of the silver was assimilated into the organism.⁶⁶ However, Loven *et al.* found no evidence that 20 nm colloidal gold crossed the daphnid gut epithelium.⁶⁷ Carbon nanotubes (CNTs) readily accumulate in the daphnid gut and are not easily excreted.^{14,15} In this present study, imaging and spICPMS showed AgNWs inside the daphnids. However, dynamic biological imaging studies will be required to determine specific route(s) of AgNW internalization.

Concluding Remarks. Our studies show that AgNWs are efficiently accumulated from media and are highly toxic to *Daphnia magna*. There is significant variation in biological response to the different AgNWs, possibly due to different uptake mechanisms or to the generation of different forms of silver within the organism, including Ag^+ , silver-rich nanoparticulates, and chemically modified internalized AgNWs. Exact pathways for AgNW absorption into *Daphnia* require further study. Short and SiO_2 -coated AgNWs were usually more toxic

than long or PVP-coated, perhaps because of the dissolution of the SiO_2 coating inside the *Daphnia*. However, these trends were not true in all growth media. Overlapping modes of toxicity include effects on the carapace and cuticle and disruption of ribosomal function. The use of sPLCPS in biologically and toxicologically relevant fluids and tissues represents a novel application for this technique that will likely have wide application in studies of metal and nanomaterial toxicity.

METHODS

Silver Nanowire Characterization. All silver nanowires (AgNWs) were purchased from nanoComposix (San Diego, CA). Stock solutions were deoxygenated by bubbling in N_2 for 1 h and were stored in rolled, lightproof bottles in an anaerobic chamber. The silver concentration of each stock solution (reported as micrograms silver per liter media ($\mu\text{g/L}$)) was measured in triplicate using inductively coupled plasma mass spectrometry (ICP-MS) after acid digestion performed by adding 100 μL of AgNW aliquots to 1.5 mL of concentrated nitric acid and storing in the dark for 2 days. Nanorod impurities were detected and quantified by removing nanowires *via* filtration and measuring total silver in filtrate with ICP-MS (Table S1). The ζ -potential measurements of short PVP- and SiO_2 -coated NWs dispersed in ultrapure water were performed using a Malvern ZetaSizer, and ζ -potential measurements could not be performed for long NWs because the size was too large nor for short NWs dispersed in growth media for which the higher ionic strength completely shielded the NW surfaces. Methods for the characterization of AgNWs with scanning transmission electron microscopy (STEM) and scanning electron microscope (SEM) and for the determination of settling rates and aggregation are detailed in the Supporting Information. TEM images of the AgNWs are found in Figures S4 and S5. Silver nitrate (99.999% trace metal basis) was obtained from Sigma-Aldrich. Bulk ICP-MS analysis of *Daphnia* growth media found no silver above detection limits.

Ionic Silver Release into Media. Ag^+ release into media and water was quantified by adding AgNWs to ultrapure water or to *Daphnia* media and measuring the dissolved silver concentration at intervals with ICP-MS. AgNWs were filtered from aliquots using a 0.02 μm pore size, 25 mm diameter syringe filter (Whatman Anotop), and the filtrate was acidified and analyzed for total silver. However, all filters effective at separating all AgNWs also significantly retained the Ag^+ ion (Figure S15). This effect was minimized by discarding the first 1 mL volume passed through the filter and averaging the Ag concentrations of three successive 1 mL filtrate volumes.

Daphnia Culture. Genetically homogeneous *Daphnia magna* originally obtained from Aquatic Research Organisms (Hampton, NH) were cultured in a growth chamber (Conviron Adaptis) at 21 °C with 16 h of light and 8 h of dark per day. Daphnids were grown in nutritive COMBO media⁶⁸ or in a moderately hard water formulation we refer to as "EPA".⁶⁹ *Daphnia* were fed *Pseudokirchneriella subcapitata* (formerly *Selenastrum capricornutum*) and yeast cereal-leaf and trout chow mix three times per week following renewal of media. Media were aerated overnight to increase dissolved oxygen levels. COMBO pH was maintained at 7.4–7.8; EPA was maintained at 7.80–8.0. Table S2 summarizes media chemical composition. The Geochemist's Workbench (Rockware) was used to predict equilibrium speciation of dissolved Ag^+ in both media, using the default database of thermodynamic constants (Table S3).

Toxicity Assays. Acute toxicity assays were conducted similarly to the U.S. EPA Whole Effluent Toxicity (WET) protocol.⁶⁹ Five first instar (<24 h old) *D. magna* were placed in 35 mL aliquots of media with different concentrations of a nanowire. At least 12 replicates of five concentrations and a media-only

control were tested for each AgNW and for Ag^+ in both media. Lethality was measured after 24 h. Acute LC_{50} values were determined using probit statistical program.⁶⁹ To determine if AgNW settling affected LC_{50} , assays were performed with and without shaking on an orbital shaker. Raw acute data for long and short PVP-NWs were compared with a *t* test (detailed in Supporting Information Methods). There was no statistical difference in daphnid lethality between still or shaken AgNW exposures ($p = 0.824$ S-PVP, 0.940 L-PVP). Subsequent exposures were done without shaking.

Transcriptomic Assays. Exposures were done with 15–20 adult (14 day old) daphnids per biological replicate at 1/10 LC_{50} in 800 mL of COMBO media for 24 h. Four biological replicates were conducted for each AgNW, for Ag^+ , and for COMBO media control. Animals were removed from exposure media, and RNA was extracted immediately in Trizol reagent (Invitrogen) with a hand-held homogenizer (Biospec Products Inc.). RNA was cleaned up with an RNeasy kit (Qiagen), and quality was assessed *via* spectrometry and on an agarose gel. Next, 300 ng of RNA was reverse-transcribed, amplified, and hybridized onto a custom Agilent oligonucleotide DNA microarray (AMADID #023710) with the Agilent Quick-Amp one-color array kit and protocol. The array contains 15 000 unique, best-responding probes from a 44 000 probe preliminary array constructed from a *Daphnia magna* expressed sequence tag database.⁷⁰ Four arrays were hybridized for each exposure condition. Arrays were scanned with a 16-bit GenePix 4000B microarray scanner with 5 μm resolution, and features were edited with GenePix Pro 6.0. Data were analyzed using a "Treatment vs. Control" design (described in detail in the Supporting Information Methods). Briefly, nonlinear trends (if any) were corrected with loess global normalization;⁷¹ differential gene expression was determined with an algorithm based on α -outlier detection procedures,⁷² and a local variance estimator based on loess was used to take heteroscedasticity into consideration.⁷² Each gene in a given "Treatment vs. Control" pair was characterized by the normalized log-transformed ratio (fold change value) and the corresponding q value (derived from p values).⁷³ All results were corrected for multiplicity of comparisons within a given "Experiment vs. Control" pair and across biological replicates. Candidate genes were annotated using Blast2GO.⁴⁴

Differential gene expression of candidate genes was confirmed with quantitative reverse transcription PCR (qPCR). Seven genes were chosen based on q value, degree of differential expression, or potential mode of toxicity. Three biological replicate RNA samples were extracted, cleaned up, and quality assessed as above. One microgram of RNA was reverse-transcribed with iScript cDNA synthesis kit (BioRad) on a Mycycler thermal cycler (Biorad). Twenty-five primer sets were tested with SsoFast amplification kit (BioRad) on a melt curve from 55 to 65 °C, and those with one qPCR product were used for subsequent analysis. qPCR amplification was performed with on a BioRad C1000 Thermal Cycler with CFX96 R-T system. Probes were designed on the NCBI online primer-designing tool (<http://www.ncbi.nlm.nih.gov/tools/primer-blast/>) and ordered from Elim Biopharm. Each gene amplification was preformed in triplicate in the control and treated RNA samples. Actin and GAPDH were used as housekeeping genes. Housekeeping cycle

threshold (C_t) value was subtracted from gene-of-interest C_t values to normalize data, and values were made linear with \log_2 transformation. Significance between control and exposed was determined by Student's t test in Excel (Microsoft) with $p < 0.05$. Primer sequences are shown in Table S5.

The Kyoto Encyclopedia of Genes and Genomes (KEGG) was used to identify biological pathways affected by exposure to Ag⁺ or to AgNW. The sequence for every gene on the microarray was subjected to a *Daphnia pulex* protein BLAST and sorted into KEGG biological pathways (www.genome.jp/kegg). Pathways representing less than 5 genes in the array were removed, leaving 95 pathways and 1402 *Daphnia pulex* homologues with an expect (E) value less than or equal to 10^{-4} . Microarray data were then input into the KEGG database and "enrichment" of differentially expressed genes (DEG) in each pathway was calculated using a modified Fisher exact probability p value.^{74,75}

Gene expression profiles were compared with hierarchical ordered partitioning and collapsing hybrid (HOPACH) cluster analysis. HOPACH analysis clusters similar gene expression profiles by computationally generating plots of similar data into a hierarchical "tree of clusters" using statistical Euclidean distance matrices.⁷⁶ Similar gene expression profiles may have similar causal mechanisms or modes of toxicity. The R package HOPACH from Bioconductor.org was applied to the gene expression data. All "NA" values were replaced with zeros. This method is a combination of divisive (top down) and agglomerative (bottom up) hierachic clustering coupled with a nonparametric bootstrap procedure, which determines the probability of cluster membership for each chemical. Cosine angle (uncentered) correlation was applied as a measure of similarity.⁷⁶

Enrichment analysis on gene expression data was performed with Blast2GO⁴⁴ (B2G) to determine molecular function over-representation in each exposure condition. Available sequences corresponding to the 15K probes on the *Daphnia magna* array were annotated with B2G with default parameters to create the reference gene set of ~2900 genes. Gene expression data were then compared to the reference set with the enrichment analysis function of B2G, using default, two-tailed settings with different false discovery rate cut-offs (0.05, 0.1, 0.15).

AgNW Exposures for splCPMS and Imaging Analyses. Two week old adult *Daphnia* were exposed to a COMBO media-only control, ionic silver (AgNO₃), or AgNWs at a silver concentration corresponding to either the LC₅₀ or 10% of the LC₅₀ value. The daphnids were exposed for 24 h, with or without food, and then transferred to silver-free medium to remove any AgNWs adhering to the carapace. Hemolymph was either collected immediately as in Mucklow *et al.*⁷⁷ or after a 1.5 h depuration period, with or without feeding (*P. subcapitata*). Briefly, daphnids were removed from the media wash and placed on a glass slide. All excess medium was removed by gentle blotting of the carapace. A 22 gauge, 1.5 in. needle was used to puncture the carapace above the heart, and the resulting bead of hemolymph was extracted with a pipet. Care was taken to avoid the intestine during removal of hemolymph and to limit unnecessary needle and pipet contact with the daphnid carapace. This method has been used in our laboratory⁷⁸ and by others for metabolomics studies⁷⁹ and is similar to other existing methods⁸⁰ that also puncture the carapace above the heart. Hemolymph was collected onto a silicon wafer for SEM imaging, described below, or into 1.5 mL Eppendorf tubes and frozen at -80 °C for storage prior to splCPMS analysis. splCPMS analysis was first done on combined samples of hemolymph from 20 animals to determine detection limits. Subsequent analyses were done on combined samples from five animals.

Scanning Electron Microscopy. Approximately 1 μL of hemolymph was pipetted onto a clean 5 × 5 mm Si wafer previously treated with a 5% H₂SO₄ solution with nochromix (GODAX Laboratories, Inc.) to create a hydrophilic surface. As hemolymph drying caused extensive precipitation of electrically insulating salt crystals, the samples were coated with graphite prior to scanning electron microscope (SEM) analysis. A JEOL SEM with backscattered electron signal was used to locate silver

particles; secondary electron signal was used for imaging. The elemental composition of imaged objects was established using the energy-dispersive X-ray (EDX) fluorescence signal. Silver was detected using the Ag K α emission line.

Dark-Field Optical Microscopy. We used a Nikon MM-400 microscope in bright-field (transmission) and dark-field (reflectance) mode to image control animals and daphnids exposed to PVP-NWs. Individual living daphnids were washed in silver-free media and imaged in a small liquid reservoir between a microscope slide and a coverslip. The reservoir was created by laying a 0.02 in. thick silicone sheet and cutting a 4 mm diameter hole. No fixative was used, as preliminary studies showed AgNWs were no longer detectable in dark-field mode following exposure to 4% paraformaldehyde. When AgNWs were located, a through-focus series determined whether they were internal or external to the organism. Images were acquired using the INFINITY Capture camera and software.

splCPMS. A Perkin-Elmer NexION 300q ICPMS with an S10 autosampler was used. For calculating nebulization efficiency, a well-characterized Au particle with narrow size distribution (British Biocell International [BBI]; 100 nm mean particle diameter) was analyzed, and the efficiency was calculated using a particle-size-based approach as described in Pace *et al.*⁸¹ Dissolved calibration solutions for sizing were made using Certi-Prep ICPMS grade standards in 2% Optima (Fisher Scientific) trace-metal-grade HCl for Au and 2% Optima trace-metal-grade HNO₃ for Ag, with the concentrations chosen such that the range of ICPMS responses would include those of the AgNW pulses. Isotopes used for analysis were Au¹⁹⁷ and Ag¹⁰⁷. Each sample run consisted of 20 000 readings, each with a dwell time of 10 ms. Nanopure water blanks were analyzed for both elements before any dissolved or particulate samples were analyzed to check for carry-over system contamination. Hemolymph controls from *Daphnia* not exposed to AgNWs were analyzed for an experimental background Ag signal. Each sample of hemolymph fluid was diluted to an appropriate particle number concentration range for analysis, typically 1000×, 5000×, or 10 000× in nanopure water (Barnstead Nanopure) to obtain sufficient volume for analysis (5 mL per run). The dilution was chosen so that ~5% of data points in a run were pulses to both generate enough pulses for a statistically valid size distribution and minimize the probability that multiple particles are detected at once. COMBO medium samples were analyzed without dilution. All dilutions were made in 15 mL Falcon polypropylene centrifuge tubes with 10 min bath sonication (Fisher, FS60H) between each dilution. Instrument tubing was changed each day before analysis to minimize contamination from previous runs and maintain a constant flow rate.

Dissolved Ag concentrations were calculated by determining a background signal and transforming this to a concentration using the dissolved Ag standards. In the case of splCPMS data containing signal from both dissolved and particulate Ag, the particulate pulses were removed from the data set by a program which calculates the average (μ) and standard deviation (s), removes any signal above $\mu + 3s$, and iterates until converging on the background and standard deviation due to dissolved Ag.³² This background is used to calculate the dissolved Ag concentration; the standard deviation is used to calculate the error in concentration.

Particle number concentrations were calculated from the number of pulses rejected from the background through the previously described iterative approach. The number of pulses was divided by the efficiency of sample transport to the plasma, the analysis time, and the flow rate and multiplied by dilution factor to yield particle number concentration.

The detection limit for dissolved Ag was calculated using the hemolymph blank signal: a calculation of three standard deviations above the blank background signal and transformation to a concentration via the dissolved Ag calibration curve yielded a detection limit of ~11 ppt. However, due to the microliter volumes of hemolymph collected for analysis and the subsequent dilution of at least 1:1000 required for splCPMS analysis, we report an effective Ag detection limit of ~10 ppb.

Conflict of Interest: The authors declare no competing financial interest.

Acknowledgment. This work was funded by the Center of Integrated Nanomechanical Systems under NSF Grant Number EEC-0832819 and by NIH Grand Opportunities (RC2) program through NANO-GO NIEHS Grant DE-FG02-08ER64613. B.G. was supported by RC2 ES018812 to C.V. Part of this work was performed at the Molecular Foundry in Lawrence Berkeley National Laboratory and was supported by the Office of Science, Office of Basic Energy Sciences, of the U.S. Department of Energy under Contract No. DE-AC02-05CH11231. We thank W. Mickelson for acquiring the TEM image of Figure 1a. We thank R. Celestre for access to the Nikon microscope.

Supporting Information Available: Table S1 estimates nanorod and ionic silver contamination in AgNW stock. Table S2 outlines *Daphnia* growth media components. Table S3 shows Ag⁺(aq) calculations in media. Table S4 lists acute LC₅₀ values of AgNWs in *Daphnia magna*. Table S5 lists qPCR primer sequences. Table S6 lists qPCR results. Table S7, in a separate file, lists differentially expressed genes. Table S8 lists affected transcripts for transporter proteins. Table S9, a separate file, displays detailed results for the Blast2GO functional enrichment analysis. Table S10 shows calculations for Ag⁺ contribution to AgNW toxicity. Figure S1 is TEM imaging of PVP-AgNW and nanorod contamination. Figure S2 shows aggregation of AgNW in solution. Figure S3 shows AgNW settling rates. Figure S4 is a TEM image showing morphological changes of the SiO₂-NW coating. Figure S5 is TEM imaging of stock AgNWs and coatings. Figure S6 is a Venn diagram showing numbers of genes expressed in-common between different exposure conditions. Figure S7 shows spICPMs data on nanowire length distribution. Figure S8 shows an AgNP precipitate in Ag⁺(aq)-exposed daphnid. Figure S9 spICPMs data on nanoparticulate silver in hemolymph following Ag⁺(aq) exposure. Figure S10 is dark-field imaging of AgNWs. Figure S11 is bright-field and dark-field imaging of the *D. magna* rostrum. Figure S12 is bright-field and dark-field imaging of the *D. magna* anterior gut. Figure S13 is bright-field imaging of the *D. magna* brood chamber. Figure S14 shows dark-field imaging of AgNWs in the *D. magna* gut. Figure S15 shows Ag⁺ retention in filters. This material is available free of charge via the Internet at <http://pubs.acs.org>.

REFERENCES AND NOTES

1. Afal, A.; Coskun, S.; Emrah Unalan, H. All Solution Processed, Nanowire Enhanced Ultraviolet Photodetectors. *Appl. Phys. Lett.* **2013**, *102*, 043503–043503.
2. Kelly, K. L.; Coronado, E.; Zhao, L. L.; Schatz, G. C. The Optical Properties of Metal Nanoparticles: The Influence of Size, Shape and Dielectric Environment. *J. Phys. Chem. B* **2003**, *107*, 668–677.
3. Yiuin-Kuen, F.; Li-Chih, L. Pattern Transfer of Aligned Metal Nano/microwires as Flexible Transparent Electrodes Using an Electrospun Nanofiber Template. *Nanotechnology* **2013**, *24*, 055301.
4. Hu, J.; Liu, Y.; Ning, C. Z.; Dutton, R.; Kang, S. M. Fringing Field Effects on Electrical Resistivity of Semiconductor Nanowire-Metal Contacts. *Appl. Phys. Lett.* **2008**, *92*, 083503–083505.
5. Law, M.; Greene, L. E.; Johnson, J. C.; Saykally, R.; Yang, P. Nanowire Dye-Sensitized Solar Cells. *Nat. Mater.* **2005**, *4*, 455–459.
6. U.S. EPA, *Nanotechnology White Paper*. U.S. EPA: Washington, D.C., 2007; Vol. EPA100/B-07/001.
7. Maynard, A. D.; Aitken, R. J.; Butz, T.; Colvin, V.; Donaldson, K.; Oberdorster, G.; Philbert, M. A.; Ryan, J.; Seaton, A.; Stone, V.; et al. Safe Handling of Nanotechnology. *Nature* **2006**, *444*, 267–269.
8. Klaine, S. J.; Alvarez, P. J.; Batley, G. E.; Fernandes, T. F.; Handy, R. D.; Lyon, D. Y.; Mahendra, S.; McLaughlin, M. J.; Lead, J. R. Nanomaterials in the Environment: Behavior, Fate, Bioavailability, and Effects. *Environ. Toxicol. Chem.* **2008**, *27*, 1825–1851.
9. Dobias, J.; Bernier-Latmani, R. Silver Release from Silver Nanoparticles in Natural Waters. *Environ. Sci. Technol.* **2013**, *47*, 4140–4146.
10. Shi, X.; von dem Bussche, A.; Hurt, R. H.; Kane, A. B.; Gao, H. Cell Entry of One-Dimensional Nanomaterials Occurs By Tip Recognition and Rotation. *Nat. Nanotechnol.* **2011**, *6*, 714–719.
11. Poland, C. A.; Duffin, R.; Kinloch, I.; Maynard, A.; Wallace, W. A.; Seaton, A.; Stone, V.; Brown, S.; Macnee, W.; Donaldson, K. Carbon Nanotubes Introduced into the Abdominal Cavity of Mice Show Asbestos-like Pathogenicity in a Pilot Study. *Nat. Nanotechnol.* **2008**, *3*, 423–428.
12. Nagai, H.; Toyokuni, S. Differences and Similarities between Carbon Nanotubes and Asbestos Fibers during Mesothelial Carcinogenesis: Shedding Light on Fiber Entry Mechanism. *Cancer Sci.* **2012**, *103*, 1378–1390.
13. Gilbert, B.; Fakra, S. C.; Xia, T.; Pokhrel, S.; Madler, L.; Nel, A. E. The Fate of ZnO Nanoparticles Administered to Human Bronchial Epithelial Cells. *ACS Nano* **2012**, *6*, 4921–4930.
14. Edgington, A. J.; Roberts, A. P.; Taylor, L. M.; Alloy, M. M.; Reppert, J.; Rao, A. M.; Mao, J.; Klaine, S. J. The Influence of Natural Organic Matter on the Toxicity of Multiwalled Carbon Nanotubes. *Environ. Toxicol. Chem.* **2010**, *29*, 2511–2518.
15. Zhu, X.; Zhu, L.; Chen, Y.; Tian, S. Acute Toxicities of Six Manufactured Nanomaterial Suspensions to *Daphnia magna*. *J. Nanopart. Res.* **2009**, *11*, 67–75.
16. Safi, M.; Yan, M.; Guudeau-Boudeville, M. A.; Conjeaud, H.; Garnier-Thibaud, V.; Boggetto, N.; Baeza-Squiban, A.; Niedergang, F.; Averbeck, D.; Berret, J. F. Interactions between Magnetic Nanowires and Living Cells: Uptake, Toxicity, and Degradation. *ACS Nano* **2011**, *5*, 5354–5364.
17. Magrez, A.; Horvath, L.; Smajda, R.; Salicio, V.; Pasquier, N.; Forro, L.; Schwaller, B. Cellular Toxicity of TiO₂-Based Nanofilaments. *ACS Nano* **2009**, *3*, 2274–2280.
18. Meng, H.; Yang, S.; Li, Z.; Xia, T.; Chen, J.; Ji, Z.; Zhang, H.; Wang, X.; Lin, S.; Huang, C.; et al. Aspect Ratio Determines the Quantity of Mesoporous Silica Nanoparticle Uptake by a Small GTPase-Dependent Macropinocytosis Mechanism. *ACS Nano* **2011**, *5*, 4434–4447.
19. Verma, N. K.; Conroy, J.; Lyons, P. E.; Coleman, J.; O'Sullivan, M. P.; Kornfeld, H.; Kelleher, D.; Volkov, Y. Autophagy Induction by Silver Nanowires: A New Aspect in the Biocompatibility Assessment of Nanocomposite Thin Films. *Toxicol. Appl. Pharmacol.* **2012**, *264*, 451–461.
20. Muller, K. H.; Kulkarni, J.; Motskin, M.; Goode, A.; Winship, P.; Skepper, J. N.; Ryan, M. P.; Porter, A. E. pH-Dependent Toxicity of High Aspect Ratio ZnO Nanowires in Macrophages Due to Intracellular Dissolution. *ACS Nano* **2010**, *4*, 6767–6779.
21. Osborne, O. J.; Johnston, B. D.; Moger, J.; Balousha, M.; Lead, J. R.; Kudoh, T.; Tyler, C. R. Effects of Particle Size and Coating on Nanoscale Ag and TiO₂ Exposure in Zebrafish (*Danio rerio*) Embryos. *Nanotoxicology* **2012**, *1*–10.
22. Poynton, H. C.; Lazorchak, J. M.; Impellitteri, C. A.; Blalock, B. J.; Rogers, K.; Allen, H. J.; Loguinov, A.; Heckman, J. L.; Govindasamy, S. Toxicogenomic Responses of Nanotoxicity in *Daphnia magna* Exposed to Silver Nitrate and Coated Silver Nanoparticles. *Environ. Sci. Technol.* **2012**, *46*, 6288–6296.
23. Schinwald, A.; Chernova, T.; Donaldson, K. Use of Silver Nanowires To Determine Thresholds for Fibre Length-Dependent Pulmonary Inflammation and Inhibition of Macrophage Migration *In Vitro*. *Part. Fibre Toxicol.* **2012**, *9*, 47–61.
24. Schinwald, A.; Donaldson, K. Use of Back-Scatter Electron Signals To Visualise Cell/Nanowires Interactions *In Vitro* and *In Vivo*; Frustrated Phagocytosis of Long Fibres in Macrophages and Compartmentalisation in Mesothelial Cells *In Vivo*. *Part. Fibre Toxicol.* **2012**, *9*, 34–47.
25. Schinwald, A.; Murphy, F. A.; Prina-Mello, A.; Poland, C. A.; Byrne, F.; Movia, D.; Glass, J. R.; Dickerson, J. C.; Schultz, D. A.; Jeffree, C. E.; et al. The Threshold Length for Fiber-Induced Acute Pleural Inflammation: Shedding Light on the Early Events in Asbestos-Induced Mesothelioma. *Toxicol. Sci.* **2012**, *128*, 461–470.
26. George, S.; Lin, S.; Jo, Z.; Thomas, C. R.; Li, L.; Mecklenburg, M.; Meng, H.; Wang, X.; Zhang, H.; Xia, T.; et al. Surface

- Defects on Plate-Shaped Silver Nanoparticles Contribute to Its Hazard Potential in a Fish Gill Cell Line and Zebrafish Embryos. *ACS Nano* **2012**, *6*, 3745–3759.
27. Hamilton, R. F.; Wu, N.; Porter, D.; Buford, M.; Wolfarth, M.; Holian, A. Particle Length-Dependent Titanium Dioxide Nanomaterials Toxicity and Bioactivity. *Part. Fibre Toxicol.* **2009**, *6*, 35–45.
 28. Ji, Z.; Wang, X.; Zhang, H.; Lin, S.; Meng, H.; Sun, B.; George, S.; Xia, T.; Nel, A. E.; Zink, J. I. Designed Synthesis of CeO₂ Nanorods and Nanowires for Studying Toxicological Effects of High Aspect Ratio Nanomaterials. *ACS Nano* **2012**, *6*, 5366–5380.
 29. Fuertes, G.; Sanchez-Munoz, O. L.; Pedrueza, E.; Abderrafi, K.; Salgado, J.; Jimenez, E. Switchable Bactericidal Effects from Novel Silica-Coated Silver Nanoparticles Mediated by Light Irradiation. *Langmuir* **2011**, *27*, 2826–2833.
 30. Baber, O.; Jang, M.; Barber, D.; Powers, K. Amorphous Silica Coatings on Magnetic Nanoparticles Enhance Stability and Reduce Toxicity to *In Vitro* BEAS-2B Cells. *Inhal. Toxicol.* **2011**, *23*, 532–543.
 31. Pace, H. E.; Rogers, N. J.; Jarolimek, C.; Coleman, V. A.; Higgins, C. P.; Ranville, J. F. Determining Transport Efficiency for the Purpose of Counting and Sizing Nanoparticles via Single Particle Inductively Coupled Plasma Mass Spectrometry. *Anal. Chem.* **2012**, *84*, 4633–4633.
 32. Mitrano, D. M.; Lesher, E. K.; Bednar, A.; Monserud, J.; Higgins, C. P.; Ranville, J. F. Detecting Nanoparticulate Silver Using Single-Particle Inductively Coupled Plasma-Mass Spectrometry. *Environ. Toxicol. Chem.* **2012**, *31*, 115–121.
 33. Tuoriniemi, J.; Cornelis, G.; Hassellov, M. Size Discrimination and Detection Capabilities of Single-Particle ICPMS for Environmental Analysis of Silver Nanoparticles. *Anal. Chem.* **2012**, *84*, 3965–3972.
 34. Reed, R. B.; Higgins, C. P.; Westerhoff, P.; Tadjiki, S.; Ranville, J. F. Overcoming Challenges in Analysis of Polydisperse Metal-Containing Nanoparticles by Single Particle Inductively Coupled Plasma Mass Spectrometry. *J. Anal. At. Spectrom.* **2012**, *27*, 1093–1100.
 35. Reed, R. B.; Ladner, D. A.; Higgins, C. P.; Westerhoff, P.; Ranville, J. F. Solubility of Nano-Zinc Oxide in Environmentally and Biologically Important Matrices. *Environ. Toxicol. Chem.* **2012**, *31*, 93–99.
 36. Han, G.; Xing, Z.; Dong, Y.; Zhang, S.; Zhang, X. One-Step Homogeneous DNA Assay with Single-Nanoparticle Detection. *Angew. Chem.* **2011**, *50*, 3462–3465.
 37. Kennedy, A. J.; Hull, M. S.; Bednar, A. J.; Goss, J. D.; Gunter, J. C.; Bouldin, J. L.; Vikesland, P. J.; Steevens, J. A. Fractinating Nanosilver: Importance for Determining Toxicity to Aquatic Test Organisms. *Environ. Sci. Technol.* **2010**, *44*, 9571–9577.
 38. Yi, D. K. A Study of Optothermal and Cytotoxic Properties of Silica Coated Au Nanorods. *Mater. Lett.* **2011**, *65*, 2319–2321.
 39. Wheeler, M. W.; Park, R. M.; Bailer, A. J. Comparing Median Lethal Concentration Values Using Confidence Interval Overlap or Ratio Tests. *Environ. Toxicol. Chem.* **2006**, *25*, 1441–1444.
 40. Edgar, R.; Domrachev, M.; Lash, A. E. Gene Expression Omnibus: NCBI Gene Expression and Hybridization Array Data Repository. *Nucleic Acids Res.* **2002**, *30*, 207–210.
 41. Bianchini, A.; Wood, C. M. Mechanism of Acute Silver Toxicity in *Daphnia magna*. *Environ. Toxicol. Chem.* **2003**, *22*, 1361–1367.
 42. Ferguson, E. A.; Leach, D. A.; Hogstrand, C. In Metallothionein Protects against Silver Blockage of Na⁺/K⁺ ATPase. 4th International Conference on Transport, Fate and Effects of Silver in the Environment; Madison, W. I., Andren, A. W., Bober, T. W., Eds.; Madison, WI, 1996; pp 191–196.
 43. Péqueux, A. Osmotic Regulation in Crustaceans. *J. Crust. Biol.* **1995**, *15*, 1–60.
 44. Conesa, A.; Gotz, S.; Garcia-Gomez, J. M.; Terol, J.; Talon, M.; Robles, M. Blast2GO: A Universal Tool for Annotation, Visualization and Analysis in Functional Genomics Research. *Bioinformatics* **2005**, *21*, 3674–3676.
 45. Lee, K. J.; Nallathamby, P. D.; Browning, L. M.; Osgood, C. J.; Xu, X. H. *In Vivo* Imaging of Transport and Biocompatibility of Single Silver Nanoparticles in Early Development of Zebrafish Embryos. *ACS Nano* **2007**, *1*, 133–143.
 46. U.S. EPA *Technical Overview of Ecological Risk Assessment*; U.S. EPA: Washington, D.C., 2012; http://www.epa.gov/oppefed1/ecorisk_ders/toera_analysis_eco.htm.
 47. Hoheisel, S. M.; Diamond, S.; Mount, D. Comparison of Nanosilver and Ionic Silver Toxicity in *Daphnia magna* and *Pimephales Promelas*. *Environ. Toxicol. Chem.* **2012**, *31*, 2557–2563.
 48. Bielmyer, G. K.; Bell, R. A.; Klaine, S. J. Effects of Ligand-Bound Silver on *Ceriodaphnia dubia*. *Environ. Toxicol. Chem.* **2002**, *21*, 2204–2208.
 49. Zhou, D.; Keller, A. A. Role of Morphology in the Aggregation Kinetics of ZnO Nanoparticles. *Water Res.* **2010**, *44*, 2948–2956.
 50. Levard, C.; Hotze, E. M.; Lowry, G. V.; Brown, G. E. Environmental Transformations of Silver Nanoparticles: Impact on Stability and Toxicity. *Environ. Sci. Technol.* **2012**, *46*, 6900–6914.
 51. Romer, I.; White, T. A.; Baalousha, M.; Chipman, K.; Viant, M. R.; Lead, J. R. Aggregation and Dispersion of Silver Nanoparticles in Exposure Media for Aquatic Toxicity Tests. *J. Chromatogr. A* **2011**, *1218*, 4226–4233.
 52. Jeon, H. J.; Yi, S. C.; Oh, S. G. Preparation and Antibacterial Effects of Ag-SiO₂ Thin Films by Sol–Gel Method. *Biomaterials* **2003**, *24*, 4921–4928.
 53. Loucaides, S.; Van Cappellen, P.; Behrends, T. Dissolution of Biogenic Silica from Land to Ocean: Role of Salinity and pH. *Limnol. Oceanogr.* **2008**, *53*, 1614–1621.
 54. Yamanaka, M.; Hara, K.; Kudo, J. Bactericidal Actions of a Silver Ion Solution on *Escherichia coli*, Studied by Energy-Filtering Transmission Electron Microscopy and Proteomic Analysis. *Appl. Environ. Microbiol.* **2005**, *71*, 7589–7593.
 55. Hollunger, G. The Effect of Trivalent Thallium on Oxidative Phosphorylation. *Acta Pharmacol. Toxicol.* **1960**, *16*, 347–356.
 56. Teodoro, J. S.; Simoes, A. M.; Duarte, F. V.; Rolo, A. P.; Murdoch, R. C.; Hussain, S. M.; Palmeira, C. M. Assessment of the Toxicity of Silver Nanoparticles *In Vitro*: A Mitochondrial Perspective. *Toxicol. in Vitro* **2011**, *25*, 664–670.
 57. Harris, A. T.; Bali, R. On the Formation and Extent of Uptake of Silver Nanoparticles by Live Plants. *J. Nanopart. Res.* **2008**, *10*, 691–695.
 58. Palomaki, J.; Valimaki, E.; Sund, J.; Vippola, M.; Clausen, P. A.; Jensen, K. A.; Savolainen, K.; Matikainen, S.; Alenius, H. Long, Needle-like Carbon Nanotubes and Asbestos Activate the NLRP3 Inflammasome through a Similar Mechanism. *ACS Nano* **2011**, *5*, 6861–6870.
 59. Jovanovic, B.; Palic, D. Immunotoxicology of Non-functionalized Engineered Nanoparticles in Aquatic Organisms with Special Emphasis on Fish—Review of Current Knowledge, Gap Identification, and Call for Further Research. *Aquat. Toxicol.* **2012**, *118*, 141–151.
 60. Bühlér, V. *Excipients for Pharmaceuticals - Povidone, Crospovidone and Copovidone*; Springer: Berlin, 2005.
 61. Ebert, D. *Ecology, Epidemiology, and Evolution of Parasitism in Daphnia* [Internet]. National Center for Biotechnology Information (US): Bethesda, MD, 2005. Available from <http://www.ncbi.nlm.nih.gov/books/NBK2036/>.
 62. Roberts, A. P.; Mount, A. S.; Seda, B.; Souther, J.; Qiao, R.; Lin, S.; Ke, P. C.; Rao, A. M.; Klaine, S. J. *In Vivo* Biomodification of Lipid-Coated Carbon Nanotubes by *Daphnia magna*. *Environ. Sci. Technol.* **2007**, *41*, 3025–3029.
 63. Johnston, B. D.; Scown, T. M.; Moger, J.; Cumberland, S. A.; Baalousha, M.; Linge, K.; van Aerle, R.; Jarvis, K.; Lead, J. R.; Tyler, C. R. Bioavailability of Nanoscale Metal Oxides TiO₂, CeO₂, and ZnO to Fish. *Environ. Sci. Technol.* **2010**, *44*, 1144–1151.
 64. Ramsden, C. S.; Smith, T. J.; Shaw, B. J.; Handy, R. D. Dietary Exposure to Titanium Dioxide Nanoparticles in Rainbow Trout (*Oncorhynchus mykiss*): No Effect on Growth, but Subtle Biochemical Disturbances in the Brain. *Ecotoxicology* **2009**, *18*, 939–951.

65. Rosenkranz, P.; Chaudhry, Q.; Stone, V.; Fernandes, T. F. A Comparison of Nanoparticle and Fine Particle Uptake by *Daphnia magna*. *Environ. Toxicol. Chem.* **2009**, *28*, 2142–2149.
66. Zhao, C. M.; Wang, W. X. Biokinetic Uptake and Efflux of Silver Nanoparticles in *Daphnia magna*. *Environ. Sci. Technol.* **2010**, *44*, 7699–7704.
67. Lovern, S. B.; Owen, H. A.; Klaper, R. Electron Microscopy of Gold Nanoparticle Intake in the Gut of *Daphnia magna*. *Nanotoxicology* **2008**, *2*, 43–48.
68. Kilham, S. S.; Kreeger, D. A.; Lynn, S. G.; Goulden, C. E.; Herrera, L. COMBO: A Defined Freshwater Culture Medium for Algae and Zooplankton. *Hydrobiologia* **1998**, *377*, 147–159.
69. U.S. EPA *Methods for Measuring the Acute Toxicity of Effluents and Receiving Waters to Freshwater and Marine Organisms*; 5th ed; U.S. EPA Office of Water: Washington, D.C., 2002.
70. Garcia-Reyero, N.; Poynton, H. C.; Kennedy, A. J.; Guan, X.; Escalon, B. L.; Chang, B.; Varshavsky, J.; Loguinov, A. V.; Vulpe, C. D.; Perkins, E. J. Biomarker Discovery and Transcriptomic Responses in *Daphnia magna* Exposed to Munitions Constituents. *Environ. Sci. Technol.* **2009**, *43*, 4188–4193.
71. Yang, Y. H.; Dudoit, S.; Luu, P.; Lin, D. M.; Peng, V.; Ngai, J.; Speed, T. P. Normalization for cDNA Microarray Data: A Robust Composite Method Addressing Single and Multiple Slide Systematic Variation. *Nucleic Acids Res.* **2002**, *30*, e15–e24.
72. Loguinov, A. V.; Mian, I. S.; Vulpe, C. D. Exploratory Differential Gene Expression Analysis in Microarray Experiments with No or Limited Replication. *Genome Biol.* **2004**, *5*, R18–33.
73. Storey, J. D.; Tibshirani, R. Statistical Significance for Genomewide Studies. *Proc. Natl. Acad. Sci. U.S.A.* **2003**, *100*, 9440–9445.
74. da Huang, W.; Sherman, B. T.; Lempicki, R. A. Systematic and Integrative Analysis of Large Gene Lists Using DAVID Bioinformatics Resources. *Nat. Protoc.* **2009**, *4*, 44–57.
75. Huang da, W.; Sherman, B. T.; Lempicki, R. A. Bioinformatics Enrichment Tools: Paths toward the Comprehensive Functional Analysis of Large Gene Lists. *Nucleic Acids Res.* **2009**, *37*, 1–13.
76. van der Laan, M. J.; Pollard, K. S. A New Algorithm for Hybrid Hierarchical Clustering with Visualization and the Bootstrap. *J. Stat. Plann. Inference* **2003**, *117*, 275–303.
77. Mucklow, P. T.; Vizoso, D. B.; Jensen, K. H.; Refardt, D.; Ebert, D. Variation in Phenoloxidase Activity and Its Relation to Parasite Resistance within and between Populations of *Daphnia magna*. *Proc. R. Soc. London, Ser. B* **2004**, *271*, 1175–1183.
78. Poynton, H. C.; Taylor, N. S.; Hicks, J.; Colson, K.; Chan, S.; Clark, C.; Scanlan, L.; Loguinov, A. V.; Vulpe, C.; Viant, M. R. Metabolomics of Microliter Hemolymph Samples Enables an Improved Understanding of the Combined Metabolic and Transcriptional Responses of *Daphnia magna* to Cadmium. *Environ. Sci. Technol.* **2011**, *45*, 3710–3717.
79. Taylor, N. S.; Weber, R. J.; White, T. A.; Viant, M. R. Discriminating between Different Acute Chemical Toxicities via Changes in the Daphnid Metabolome. *Toxicol. Sci.* **2010**, *118*, 307–317.
80. Gerke, P.; Bording, C.; Zeis, B.; Paul, R. J. Adaptive Haemoglobin Gene Control in *Daphnia pulex* at Different Oxygen and Temperature Conditions. *Comp. Biochem. Physiol., Part A: Mol. Integr. Physiol.* **2011**, *159*, 56–65.
81. Pace, H. E.; Lesher, E. K.; Ranville, J. F. Influence of Stability on the Acute Toxicity of CdSe/ZnS Nanocrystals to *Daphnia Magna*. *Environ. Toxicol. Chem.* **2010**, *29*, 1338–1344.